Reliability Engineering and System Safety 188 (2019) 155–167

Contents lists available at ScienceDirect

Reliability Engineering and System Safety

journal homepage: www.elsevier.com/locate/ress

Assessing the accessibility of petrochemical facilities during storm surge events

Carl Bernier[a], Ioannis Gidaris[b], Georgios P. Balomenos[c], Jamie E. Padgett[a,*]

[a] Department of Civil and Environmental Engineering, Rice University, Houston, TX 77005, USA
[b] Catastrophe Perils, Swiss Re, Armonk, NY 10504, USA
[c] Department of Civil Engineering, McMaster University, Hamilton, Ontario L8S 4L7, Canada

ARTICLE INFO

Keywords:
Storm surge
Road network
Bridges
Storage tanks
Accessibility analysis
NaTech

ABSTRACT

Recent hurricane events have exposed the susceptibility of petrochemical facilities to severe transportation network disruptions due to flooding or storm surge. Network disruptions can result in cascading impacts or amplify the consequences of damage to petrochemical infrastructure due to delayed emergency response and limited access to the site. This study presents a scenario-based framework to assess the accessibility of petrochemical facilities by emergency responders and workers during storm surge events. First, the framework couples storm surge modeling with aboveground storage tank fragility models to determine the locations where natural hazard-triggered technological (NaTech) events could occur. Then, storm surge modeling is coupled with bridge fragility models and geographic system analysis to evaluate the potential for network disruptions such as bridge failures and road inundations. Finally, probabilistic network analyses are performed to evaluate the time-evolving accessibility of NaTech sites to emergency responders and facility workers. As a proof of concept, the framework is applied to a case study area. Results for the case study area demonstrate that the proposed framework is a powerful tool to quantify the accessibility of potential NaTech events, facilitate mitigation and emergency activities, and improve the management of critical resources and personnel during and after a storm.

1. Introduction

Due to their location in coastal areas, petrochemical facilities are often exposed to natural hazards such as flooding and storm surge. As a consequence, petrochemical infrastructure, especially aboveground storage tanks (ASTs), have suffered damage resulting in the release of hazardous chemicals (i.e. NaTech events) during almost every major storm event in the US since 1990 [1]. During Hurricanes Katrina and Rita, damage to petrochemical infrastructure caused the release of more than 30 million liters of hazardous chemicals [2]. More recently, during Hurricane Harvey, at least 2 million liters of hazardous chemicals were spilled as a result of damage to petrochemical infrastructure [3]. Such spills can result in severe environmental impacts to wildlife and sensitive ecosystems as well as economic impacts due to cleanup costs, lawsuits, and disruption of port activities. Moreover, as petrochemical facilities are often located in developed areas, spills can have profound effects on the mental and physical wellbeing of nearby communities [4].

While storm surge and flooding are often the direct cause of NaTech events [5,6], these hazards can also significantly hamper mitigation and emergency activities that could prevent such NaTech events from happening or limit their potentially disastrous consequences [7]. Flood and storm surge events are generally widespread and can lead to severe transportation network disruptions, thereby restricting the accessibility of petrochemical facilities. In turn, such accessibility losses can result in cascading impacts, potentially culminating in a NaTech event, due to the inability to perform critical mitigation activities, and can also amplify the impacts of a NaTech event due to delayed emergency response and limited access to the site [7–10]. For instance, during Hurricane Harvey, severe flooding at a major oil terminal in the Houston region hindered emergency personnel's access to two damaged ASTs for almost five days, resulting in a spill of approximately 1.75 million liters of gasoline [11]. After Harvey, several industry managers also reported issues regarding the ability to bring in workers and contractors to cleanup sites, repair and maintain critical infrastructure as well as to restart operations [12].

An adequate assessment of the effects of transportation network disruptions on mitigation and emergency activities first requires tools to

* Corresponding author.
E-mail addresses: carl.bernier@rice.edu (C. Bernier), gidaris31@gmail.com (I. Gidaris), balomeng@mcmaster.ca (G.P. Balomenos), jamie.padgett@rice.edu (J.E. Padgett).

https://doi.org/10.1016/j.ress.2019.03.021
Received 25 September 2018; Received in revised form 24 January 2019; Accepted 3 March 2019
Available online 05 March 2019
0951-8320/

evaluate the accessibility of petrochemical facilities during and after storm events. In recent years, several studies have proposed frameworks to evaluate and quantify road network accessibility during flood or storm events. Coles et al. [13] presented a method that coupled flood modeling with network analysis to assess the impacts of flooding on emergency response times in the city of York in the United Kingdom (UK). Using a similar approach, Green et al. [14] assessed the impacts of flooding on emergency responder operations in the city of Leicester, UK, while Yin et al. [15] evaluated the cascading impacts of storm surge on emergency response times in the city of New York, US. Following Hurricane Harvey, Gori et al. [16] also proposed a framework to assess the evolution of road network accessibility and recovery during flood events in Houston, US. While these studies provided useful methods to evaluate the accessibility of urban areas during surge or flood events, they are not directly applicable for petrochemical infrastructure because they cannot identify the potential sites that emergency responders might need to access. Given the potentially large number of exposed petrochemical infrastructure during a storm event, it is essential to determine the locations of vulnerable infrastructure and the likelihood of a NaTech event at these locations to efficiently manage emergency resources. Moreover, these studies considered road inundation as the only source of disruption, neglecting the potential failures of critical transportation infrastructures, such as bridges, which could further disrupt transportation networks even when floodwaters have receded. Finally, these studies mainly used deterministic approaches, neglecting various sources of uncertainty, which can significantly affect accessibility and emergency activities.

The objective of this paper is to develop a comprehensive framework to first identify the potential locations of NaTech events and then evaluate the accessibility of these NaTech events during and after a storm surge event while explicitly considering the structural vulnerability of transportation infrastructure and the uncertainties associated with network disruptions. This framework integrates storm surge modeling, AST fragility modeling, coastal bridge fragility modeling, and network analysis to determine the time-evolving accessibility of NaTech sites to emergency responders as well as the ability of workers to access the facilities after a storm. This framework also relies on Monte Carlo simulation (MCS) to propagate the uncertainties associated with bridge vulnerability, speed of emergency vehicles, and inundation threshold for road closures in the accessibility analysis. As a proof of concept, the proposed framework is applied to a case study area located along the Houston Ship Channel, in Texas, US.

The next sections of this paper detail the development and application of the proposed framework. Section 2 presents the integrated framework and the major components of the framework. Specifically, this section details the storm surge modeling, the vulnerability assessment of ASTs and bridges subjected to storm surge in order to identify the potential locations of NaTech events as well as the potential for bridge failures, the network accessibility analysis methodology, and the propagation of uncertainties in the analysis. The case study area and the storm surge scenarios adopted to illustrate the application of the integrated framework are introduced in Section 3. Results of the accessibility analysis for the case study area are then presented and discussed in Section 4. Finally, Section 5 summarizes the major conclusions and potential future work.

2. Methodology

2.1. Overview of the proposed integrated framework

In order to assess the accessibility of petrochemical facilities during storm surge events, this study relies on a scenario-based framework coupling storm surge modeling, AST vulnerability modeling, coastal bridge vulnerability modeling, GIS analysis, and probabilistic network analysis. An overview of the proposed integrated framework is shown in Fig. 1 along with links between different components of the framework and tools used for each component. First, storm surge modeling helps determine the time evolution of surge depth and extent in the area of interest for a given storm scenario. While the framework could also consider flood events, this study specifically focuses on storm surge, which has historically caused more significant damage to petrochemical and integrated transportation infrastructure than flooding [1,17]. Results of the storm surge modeling are then coupled with fragility models to determine the vulnerability of ASTs in the area of interest. The probability of failure of each tank subjected to storm surge is evaluated to determine the potential locations of NaTech events in the network as well as the time period when NaTech events are most likely to occur during the storm scenario. The petrochemical infrastructure considered herein are limited to ASTs, which are the most commonly damaged infrastructure during storm surge events and are also responsible for the largest spills during such events [2,18].

Results of the storm surge modeling are also used to evaluate potential disruptions in the road network due to bridge failure and road inundation. At a given time instant during a storm, the potential for bridge failure is assessed through the use of fragility models for coastal bridges. The failure or not of a specific bridge is modeled as a Bernoulli trial given its probability of failure; if a bridge fails, it is removed from the road network. As detailed later, Markov chains are also used to account for the fact that bridge failure could have occurred during a previous time instant of the storm. Even though other transportation infrastructure, such as roads, could also suffer damage during storm surge, this study only considers the structural vulnerability of bridges due to the limited availability of road fragility models and because bridges are often considered to be among the most vulnerable components of transportation systems during storms [19,20]. Nonetheless, the potential for road closures due to inundation is still considered in the framework. At a given time, if the depth of water on a road is higher than an inundation threshold (Θ), the road is assumed to be closed and is removed from the road network. The depths of water on the roads are obtained through a GIS analysis that intersects road locations and elevations with surge elevations. Bridge inundation is also considered because a bridge could be closed due to high water without necessarily failing. Previous studies in the US have proposed a deterministic value of 0.6 m for Θ [16,21] as most vehicles can be carried away by 0.6 m of water [22]. However, there are major sources of uncertainty regarding Θ. Emergency vehicles might be able to travel in higher waters. Moreover, drivers may not be aware of the exact depth of water on a road; some may perceive a road to be inaccessible even though there is less than 0.6 m of water, while others could perceive the opposite. Thus, this study considers Θ as a random variable; a truncated normal distribution ($\pm$ 2 standard deviation) with a mean of 0.6 m and a standard deviation of 0.075 m is assumed for Θ.

With knowledge of the potential disruptions in the road network at a time instant, the network accessibility analysis is performed next by using network and graph theories as well as Monte Carlo simulations (MCS) to consider the probabilistic nature of bridge failures and propagate uncertainties associated with the inundation threshold and vehicle speed. The accessibility of the previously identified NaTech sites to emergency responders is then assessed by computing four metrics, detailed in Section 2.6.: (i) connectivity loss; (ii) probability of non-connectivity; (iii) travel time; and (iv) travel distance. Finally, this process is repeated for various time instants of the storm scenario to (a) evaluate the time evolution of the accessibility of NaTech sites to emergency responders, and (b) determine the accessibility of the facilities to workers to repair critical infrastructure and restart operations after a storm. When performing the accessibility analysis, the effects of traffic conditions, traffic directions, and traffic signals are neglected; these assumptions are reasonable as no traffic is expected during a severe storm, and emergency responders would be exempted from driving regulations such as traffic signals and one-way roads. Additional details regarding the components of the integrated framework are provided in the subsequent sections.

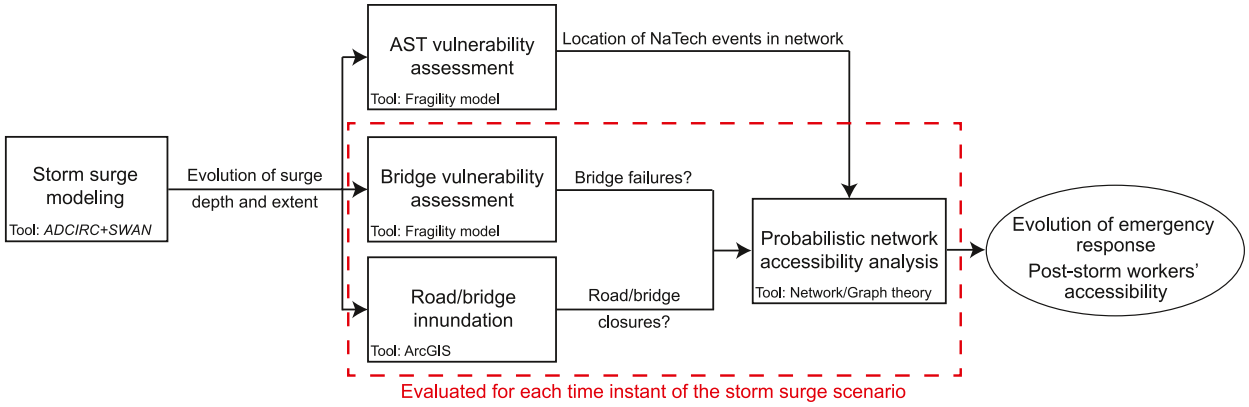

Fig. 1. Overview of the integrated framework.

2.2. Data requirements

Before applying the integrated framework to a case study area, various sources of data must be gathered in order to obtain an adequate representation of the road network, evaluate the vulnerability of ASTs and bridges, and perform the accessibility analysis. First, the development of the road network requires collection of, in GIS format, the location and elevation of: (i) highways and roads in the area of interest; (ii) bridges; (iii) emergency services, such as fire stations or any other services that would respond to a NaTech event; (iv) ASTs; and (v) residential neighborhoods where facilities' workers are residing. To adequately assess their vulnerability, the geometry and design details of each of the ASTs and bridges in the area of interest are also required. Finally, to estimate travel times in the network, the speed of vehicles (S) on the road segments is required. The speed of vehicles is considered as a random variable to account for uncertainties. Again, a truncated normal distribution (± 2 standard deviation) is employed. The mean of the truncated normal distribution is defined as the speed limit of the road segment minus 10 mph (16 km/h) to account for adverse driving conditions during a storm [16]; a standard deviation of 5 mph (8 km/h) is assumed.

2.3. Storm surge modeling

The first step of the integrated framework involves determining surge conditions in the area of interest. The framework specifically relies on scenario-based hazard models to evaluate the vulnerability of ASTs and determine disruptions in the network. Thus, the results of the framework are only representative of the storm scenario under consideration. In future work, such a framework could theoretically be coupled with probabilistic hazard models, with the caveat that the integration as presented requires knowledge of the temporal evolution of storm surge which is not typically retained in probabilistic models of storm events. The storm scenarios are modeled here using the Advanced Circulation (*ADCIRC*) and the Simulating Waves Nearshore (*SWAN*) computer programs. For a given meteorological forcing (i.e. wind velocity and atmospheric pressure), which can correspond to a historic or synthetic event, *ADCIRC + SWAN* simultaneously solve surge elevations, currents, wave periods, and significant wave heights (H_s) to predict the time evolution of surge and wave conditions [23]. *ADCIRC + SWAN* are well validated against historical storms in the US [24]. To perform the analyses presented in the next sections, time histories of surge and wave conditions at each AST and bridge location as well as time histories of water depth on each road segment in the area of interest are extracted for a given storm scenario using *ArcGIS* [25]. *ADCIRC + SWAN* results are typically output with a time step of 1 h

2.4. Vulnerability assessment of ASTs during storm surge

Once the surge conditions are known for a given storm scenario, it is possible to assess the structural vulnerability of ASTs in order to determine (i) the potential locations of NaTech events in the area of interest, as well as (ii) the time period when emergency responders might need to respond to NaTech events. ASTs are a critical component of petrochemical facilities for the storage of raw and refined products. ASTs are generally constructed from welded thin steel plates forming a vertical cylinder. While this design makes them lightweight and able to withstand internal pressure, it also leaves them vulnerable to storm surge. Two failure mechanisms are possible during storm surge events: (i) flotation due to buoyancy forces [26]; and (ii) buckling of the tank shell due to excessive water pressure [18]. To assess the structural vulnerability of ASTs, the integrated framework relies on parametrized fragility models. Parametrized fragility models provide the conditional probability of failure as a function of the structure characteristics and the loads acting on it. Such fragility models are useful tools to perform vulnerability assessment as they can be readily applied for any AST geometry, internal liquid properties, and surge conditions.

The fragility models developed by Kameshwar and Padgett [27] for unanchored and anchored ASTs are employed here. These fragility models are parametrized on the AST diameter (D), height (H), internal liquid height (L), internal liquid density (ρ_L), steel design stress (S_d), external surge height acting on the AST (h), and an additional set of parameters $\boldsymbol{X_a}$ if the AST is anchored to the ground. The surge height (h) defines the load intensity from the storm surge. The fragility models were derived for surge conditions representative of the US Gulf Coast and by considering both flotation and buckling as potential failures modes. Based on these models, the probability of failure of an AST subjected to storm surge is given by a logistic regression equation as shown in Eq. (1).

$$P(\text{Failure}|D, H, L, \rho_L, S_d, h, \mathbf{X}_a) = \frac{1}{1 + \exp(-l(D, H, L, \rho_L, S_d, h, \mathbf{X}_a))} \quad (1)$$

In this equation, $l(\cdot)$ = logit functions that express the odds of failure for a combination of D, H, L, ρ_L, S_d, h, and $\boldsymbol{X_a}$ values. The logit functions employed in this study are the ones found in Kameshwar and Padgett [27] for unanchored and anchored ASTs.

By knowing an AST geometry (D and H), its design (S_d and $\boldsymbol{X_a}$), its internal liquid (L and ρ_L), and the surge height (h) acting on the AST, it is possible to estimate directly the probability of failure by evaluating Eq. (1). However, prior to a storm, the precise internal liquid height and the exact content stored in a tank are generally unknown, and these two parameters should be considered as sources of uncertainty and treated as random variables. The probability of failure is then obtained by convolving Eq. (1) over the probability density functions (PDFs) of L

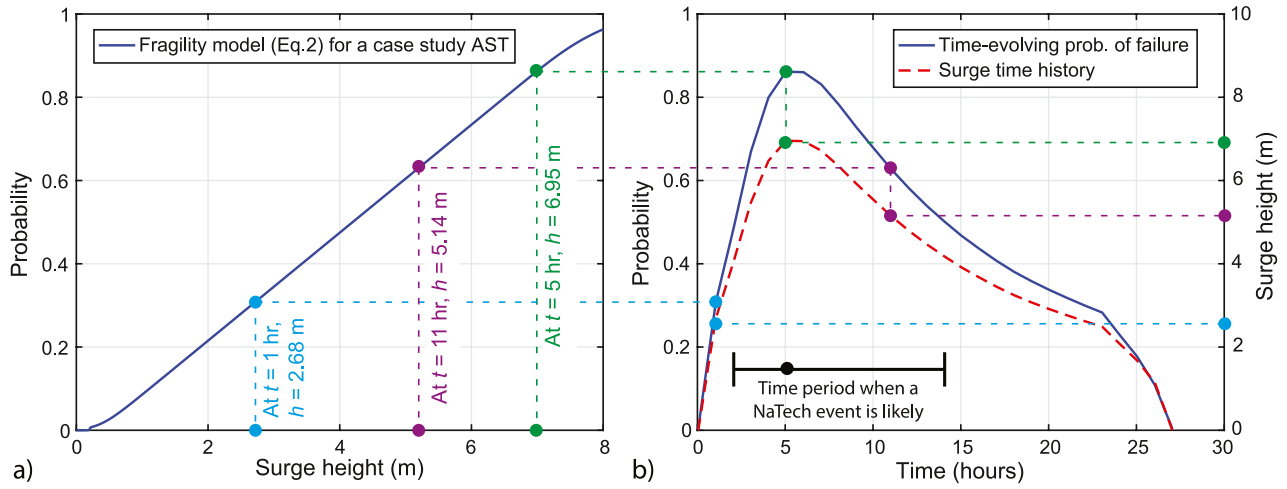

Fig. 2. Example of: (a) fragility curve; and (b) time-evolving probability of failure for a case study unanchored AST with $D = 18.3$ m, $H = 11.5$ m, $B = 0$ m, and $S_d = 160$ MPa.

and ρ_L as shown in Eq. (2).

$$P(\text{Failure}|D, H, S_d, h, B, \mathbf{X}_a) = \begin{cases} \int_L \int_{\rho_L} P(\text{Failure}|D, H, L, \rho_L, S_d, h, \mathbf{X}_a) f_L(l) f_{\rho_L}(\rho_l) \mathrm{d}\rho_L \mathrm{d}L & h > B \\ 0 & h \le B \end{cases} \quad (2)$$

In this equation, $f_L(l)$ and $f_{\rho_L}(\rho_l)$ = PDFs of L and ρ_L respectively; L is considered as uniformly distributed with bounds of 0 and $0.9H$ [28], while ρ_L is also uniformly distributed with bounds of 700 and 950 kg/m^3, which cover most products stored in a petrochemical facility. Eq. (2) also consider the presence of a containment berm around an AST, which can prevent damage as long as the berm height (B) is greater than h. Eq. (2) can be solved via MCS or numerical integration.

For a given AST (i.e., fixed values for D, H, S_d, B, and $\boldsymbol{X_a}$), Eq. (2) can also be evaluated for an increasing value of h to obtain a fragility curve as shown in Fig. 2a. Such a curve is then useful to compute the time-evolving probability of failure of an AST during a storm scenario. Storm events generally last for a few days, and the probability of failure will vary in time as the surge increases and then recedes. Since the fragility models are parametrized on the surge depth acting on an AST rather than the storm intensity, it is possible to evaluate the probability of failure at any time instant t of a storm scenario. As illustrated in Fig. 2b, the surge height at time t ($h^{(t)}$) is first extracted from the storm surge modeling, the corresponding probability of failure is then estimated, and the process is repeated for all time steps of a storm scenario to obtain the time-evolving probability of failure of an AST. Additional details on the concept of time-evolving probability of failure can be found in Masoomi et al. [29], while additional details on the fragility models and their usage can be found in Kameshwar and Padgett [27].

By computing the time-evolving probability of failure of all ASTs in the area of interest, the locations of ASTs likely to fail and trigger a NaTech event during a storm scenario can then be identified; ASTs for which the probability of failure reach above 0.5 are considered herein as likely to fail. Also, it is possible to identify: (i) the time period during a storm scenario when a failure is likely to happen and emergency responders might need access, which corresponds to the period when the probability of failure remains above 0.5 as shown in Fig. 2b; and (ii) the most likely point in time for failure, which corresponds to the time when the probability of failure is maximum.

2.5. Vulnerability assessment of bridges during storm surge

With the storm surge modeling results, it is also possible to assess the structural vulnerability of bridges in order to evaluate disruptions in the road network due to bridge failures. Bridges are a vital component of transportation networks; their failure can result in severe transportation disruptions, both because they are often the only network links to cross waterways or other major obstacles and they require long periods of time to repair [19]. Previous storm events have highlighted the structural vulnerability of bridges subjected to storm surge, with bridge deck unseating being the dominant failure mode [19,30]; deck unseating occurs due to the buoyant and pounding forces from the surge and wave loads. As for ASTs, the vulnerability assessment of bridges is performed using parametrized fragility models. Balomenos et al. [31] recently developed fragility models to estimate the probability of deck unseating for the four main types of bridge spans found in the US Gulf Coast region (i.e. steel girder, concrete girder, slab, and box girder). Based on a logistic regression model, the probability of unseating of a bridge span is:

$$P(\text{Unseating}|Z_c, H_{max}, s_p, \mathbf{X}) = \frac{1}{1 + \exp(-l(Z_c, H_{max}, s_p, \mathbf{X}))} \quad (3)$$

where Z_c = relative surge height, which corresponds to the deck elevation minus the surge elevation at the bridge location; H_{max} = maximum wave height, which is calculated from H_s at the bridge location as detailed below; s_p = factor to consider the spatial variability of the waves, which takes a value between 0 and 1 according to the proportion of the span that is actually affected by surge and wave loads; $\boldsymbol{X}$ = vector of parameters describing the structural characteristics of the span such as the span length and width, and other parameters depending on the type of superstructure; and $l(\cdot)$ = logit functions that can be found in Balomenos et al. [31] for the four bridge span types.

Because Eq. (3) provides the probability of failure of a single span, it does not reflect the structural vulnerability of a bridge. Bridges can be composed of multiple spans with different structural characteristics, and the loads acting on each span are different as waves are spatially variable. The probability of failure of a bridge can be modeled using a series system assumption as shown in Eq. (4). This equation indicates that the failure of a bridge occurs if at least one span is unseated.

$$P(\text{Failure}|Z_c, H_{max}) = P\left(\bigcup_{i=1}^{N_{sp}} (\text{Unseating}_i|Z_c, H_{max}, s_{p,i}, \mathbf{X}_i)\right) \quad (4)$$

In the above equation, N_{sp} = number of spans; Unseating_i = unseating of the ith span, modeled as a Bernoulli trial with probability of unseating obtained from Eq. (3) and the adequate logit function according to the span type; $s_{p,i}$ = proportion of the ith

span subjected to surge and wave loads; and $\boldsymbol{X}_i$ = structural characteristic of the ith span. Eq. (4) is evaluated here by using the MCS-based methodology detailed in Balomenos et al. [31].

Once the values of Z_c and H_{max} at a given time step t of a storm scenario are known, it is possible to use Eq. (4) to estimate the probability of failure of a bridge at time t. However, in order to evaluate network disruption due to a bridge failure, consideration must be given to the fact that (i) failure could have occurred at a previous time step, and (ii) once a bridge fails, it will remain in a failed state until it is repaired. By assuming a discrete Markov process, the probability that a bridge is in a failed state at time t, while it was initially, at time 0, in a safe state, and that failure could have occurred at any time step between 0 and t, can be expressed as:

$$p_f^{(t)} = P(\text{Failed state at } t \mid \text{Safe state at } 0) = 1 - \prod_{j=1}^{t} (1 - P(\text{Failure}|Z_c^{(j)}, H_{\max}^{(j)})) \quad (5)$$

where $Z_c^{(j)}$ = relative surge height at jth time step, $H_{max}^{(j)}$ = maximum wave height at jth time step, and $P(\text{Failure} \mid Z_c^{(j)}, H_{max}^{(j)})$ is evaluated from Eq. (4). According to Markov chain theory [32], Eq. (5) is the n-step ($n = t$ here) transition probability of going from a safe state to a failed state, while Eq. (4) evaluated at time step t is simply the transition probability of going from a safe state to a failed state between time steps t-1 and t. This assumes that Eq. (4) provides a probability of failure over a period of one hour, which corresponds to the time step of the storm surge modeling results. The values of H_{max} used in Eq. (4) are selected to be representative of the maximum wave height that could be observed during a one hour period according to the H_s values obtained from the storm surge modeling and the distribution of wave height proposed by Elfrink et al. [33]. Moreover, Eq. (5) assumes that it is not possible to go from a failed state to a safe state. This assumption is adequate given the time scale of this study; it is unlikely that a bridge will be repaired or restored within a day of a storm. However, this assumption would need to be reconsidered if a larger time scale was examined. Fig. 3 shows an example of the time-evolving probability of failure (Eq. (4)) and probability of being in a failed state (Eq. (5)) for a single span concrete girder bridge.

2.6. Road network accessibility analysis

With knowledge of the potential NaTech events and bridge failures, the last component of the integrated framework consists of the quantification and assessment of emergency response accessibility through a network analysis. First, the sources of data listed in Section 2.2. are mapped in *ArcGIS* to construct the road network, which is composed of links and nodes. The network links correspond to road segments, while the network nodes correspond to road segment intersections, bridge locations, emergency service stations, and NaTech event locations. Then, to perform the network analysis, a mathematical representation of the road network is obtained. This mathematical representation is depicted using network theory concepts [34], and in particular by representing the topology of a network as a graph $G = (V,E)$, where $V = \{v_1, \ldots, v_n\}$ and $E = \{e_1, \ldots, e_m\}$ are sets of n nodes and m links, respectively. Any graph G with n nodes can then be represented by its $n \times n$ adjacency matrix ($\mathbf{A}$), where $A_{ij} = 1$ if there is a link directly connecting v_i to v_j ($i \neq j$) and $A_{ij} = 0$ otherwise [34,35]. The A_{ij} values can be obtained by extracting the edge list of the road network in *ArcGIS*. The edge list corresponds to a list of all of the network's links as well as the nodes that are connected. As all links are two-way roads, the adjacency matrix is symmetric (i.e., $A_{ij} = A_{ji}$). The concepts of an edge list and adjacency matrix are illustrated in Fig. 4a through a simple graph as an example representing a network that has not sustained any disruptions yet. Fig. 4b also presents the effects of network disruptions on the edge list and adjacency matrix and is further discussed in the next paragraphs.

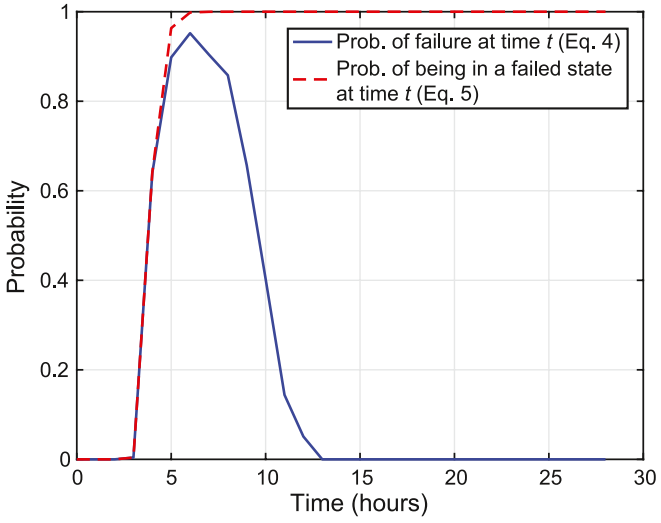

Fig. 3. Example time evolution of the probability of failure of a bridge.

The previous mathematical representation of a network is binary (i.e. the links form simple on/off connections between the nodes). However, in some cases it is useful to represent links as having a weight to them. Such weighted networks can be represented by giving the elements of the adjacency matrix values equal to the weights of the corresponding connections [34]. In road transportation networks, it is common to use the road link length and road link travel time as weights such that quantities like shortest (i.e., minimum distance covered) and quickest (i.e., minimum travel time required) paths between two nodes of interest can be evaluated. Here, these two choices are adopted as link weights w_{ij}, with the link length l_{ij} calculated in *ArcGIS* and the travel time t_{ij} estimated as $t_{ij} = l_{ij}/s_{ij}$, where s_{ij} denotes the estimated vehicle speed for each network link ij connecting nodes v_i and v_j. For each link, s_{ij} is sampled from the vehicle speed (S) probability distribution presented in Section 2.2.

After the undisrupted network is mathematically represented by $\mathbf{A}$ and w_{ij}, the accessibility between an origin node (O) and a destination node (D) as well as the effects of network disruptions on accessibility are quantified by using the methodology summarized in Fig. 5. This figure presents an overview of the Monte Carlo-based network accessibility analysis at a given time step t during a storm scenario. In the integrated framework, the origin nodes correspond to the location of emergency responders or workers, while the destination nodes correspond to the location of NaTech events identified in the AST vulnerability assessment part of the framework.

For a given MCS sample, the water depth ($h^{(t)}$) on each road link as well as the relative surge height ($Z_c^{(t)}$) and maximum wave height ($H_{max}^{(t)}$) at each bridge location at time t are extracted in *ArcGIS* as previously detailed in Section 2.3. The potential for closed roads and failed bridges is then evaluated using the indicator functions shown in Eqs. (6) and (7).

$$\text{I[Closed road/bridge]} = \begin{cases} 1 & \text{if } h^{(t)} \geq \theta \\ 0 & \text{if } h^{(t)} < \theta \end{cases} \quad (6)$$

$$\text{I[Failed bridge]} = \begin{cases} 1 & \text{if } p_f^{(t)} \geq u \\ 0 & \text{if } p_f^{(t)} < u \end{cases} \quad (7)$$

In these equations, θ = threshold sampled from the inundation threshold (Θ) probability distribution presented in Section 2.1, u = random number sampled from a uniform distribution with lower and upper bounds of 0 and 1, and $p_f^{(t)}$ is evaluated from Eq. (5). Eq. (7) indicates that the likelihood of a bridge being in a failed state is

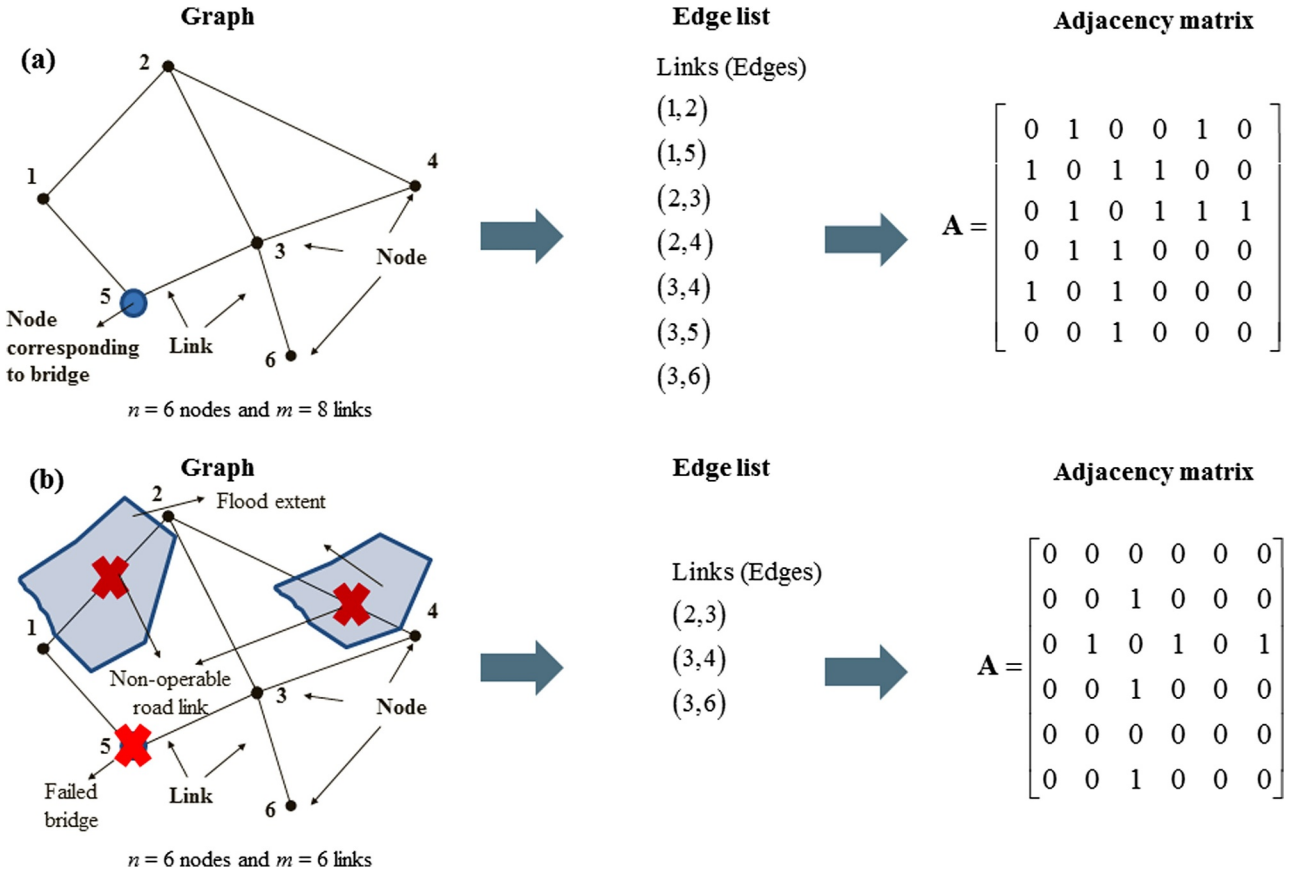

Fig. 4. (a) Example graph with edge list and adjacency matrix (A) representation [34]; and (b) effects of surge-induced disruptions on the adjacency matrix.

modeled as a Bernoulli trial. For bridges, Eq. (6) is also verified with $h^{(t)} = -Z_c^{(t)}$ to determine if the bridge could be closed due to inundation even though it did not fail from deck unseating. If a road is closed, its corresponding link is removed from the edge list; if a bridge is closed or failed, all the links connected to the bridge node are removed from the edge list. The A_{ij} elements of the adjacency matrix are then modified accordingly as illustrated in Fig. 4b for a simple network.

The network analysis is then performed with the modified adjacency matrix of the MCS sample by solving the shortest-path problem [36] using the Dijkstra's algorithm [37] with weights w_{ij} equal to l_{ij} and t_{ij} to determine the shortest and quickest paths, respectively, between nodes O and D. For the MCS sample, the accessibility between nodes O and D at time t is then quantified by computing the four following metrics:

(i) Connectivity loss ($CL_{O\to D}^{(t)}$): This metric corresponds to a measure of the efficiency reduction when traveling from nodes O to D on the disrupted framework and is expressed as:

$$CL_{O\to D}^{(t)} = 1 - L_{O\to D}^{(t=0)}/L_{O\to D}^{(t)};\quad 0 \le CL_{O\to D}^{(t)} \le 1 \tag{8}$$

where and $L_{O\to D}^{(t)}$ = lengths of the shortest OD path for the undisrupted network at time 0 and disrupted network at time t. The metric $CL_{O\to D}^{(t)}$ is continuous between 0 and 1, with $CL_{O\to D}^{(t)} = 0$ corresponding to the case where the disruptions do not affect the path between O and D, and $CL_{O\to D}^{(t)} = 1$ corresponding to the case where no path exists between O and D.

(ii) Probability of non-connectivity ($P_{f,O\to D}^{(t)}$): This metric indicates the probability of existence of a path between nodes O and D and is expressed as the following indicator function:

$$P_{f,O\to D}^{(t)} = \mathrm{I}[\text{OD path}] = \begin{cases} 1 & \text{if OD path exists} \\ 0 & \text{if no OD path exists} \end{cases} \tag{9}$$

Although $CL_{O\to D}^{(t)}$ and $P_{f,O\to D}^{(t)}$ may look like similar metrics, they provide very different information regarding accessibility performance as detailed in the next section.

(iii) Travel time ($T_{O\to D}^{(t)}$): This metric corresponds to the minimum travel time between nodes O and D on the disrupted road network. The minimum travel time is calculated by summing the weights $w_{ij} = t_{ij}$ of the road links comprising the quickest path between O and D. The t_{ij} values are obtained by sampling the s_{ij} values from the vehicle speed (S) probability distribution, as described previously.

(iv) Travel distance ($L_{O\to D}^{(t)}$): This metric corresponds to the minimum travel distance between nodes O and D on the disrupted road network. The minimum travel distance is calculated by summing the weights $w_{ij} = l_{ij}$ of the road links comprising the shortest path between O and D.

In addition to the four previous accessibility metrics, another metric, the operational path ratio (r), is also computed to evaluate the overall effects of surge-induced disruptions on the performance of the entire road network (i.e. not only between the selected O and D nodes). The operational path ratio at time step t is evaluated as:

$$r^{(t)} = N_{disrupted}^{(t)}/N_{undisrupted} \tag{10}$$

where $N_{disrupted}^{(t)}$ = number of all possible operable paths between any pair of nodes in the disrupted network at time t and $N_{undisrupted}$ = number of all possible operable paths between any pair of nodes in the undisrupted network (i.e., before the storm).

In order to consider the probabilistic nature of Θ, S, and $p_f^{(t)}$ in the network analysis, the above procedure is repeated for a total of N_{sims} samples; a total of 10,000 samples is used here. The above metrics are first computed independently for each MCS sample and then statistics of the metrics, such as the mean values (i.e., $\overline{CL}_{O\to D}^{(t)}$, $\overline{P}_{f,O\to D}^{(t)}$, $\overline{T}_{O\to D}^{(t)}$, $\overline{L}_{O\to D}^{(t)}$, and $\overline{r}^{(t)}$) and the confidence bounds, are computed. The confidence bounds are obtained by extracting the adequate percentile values from the MCS samples (e.g., the 90% confidence bounds

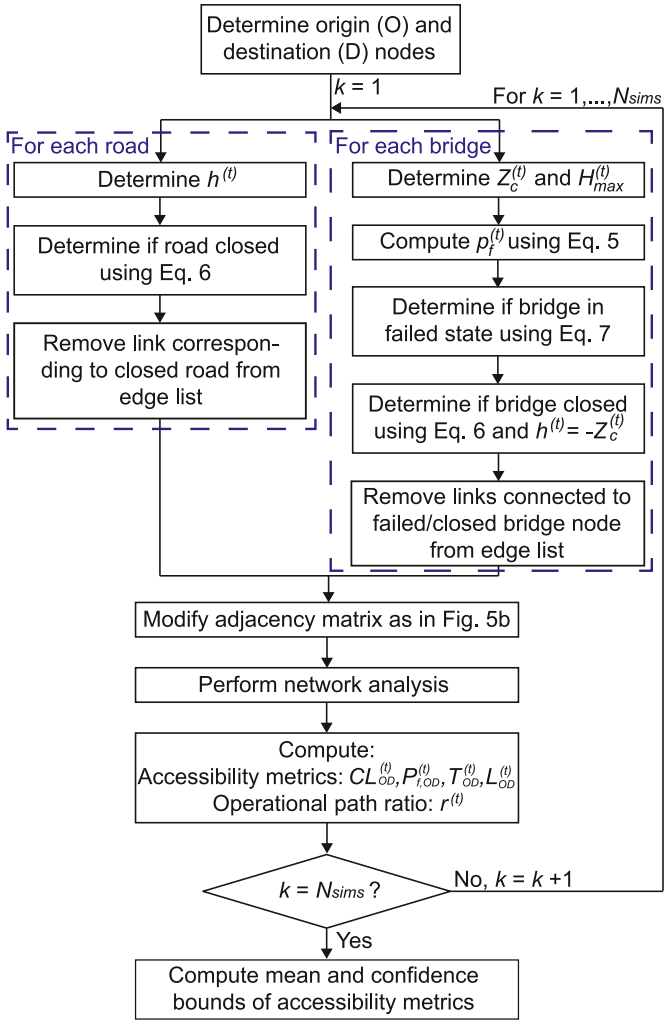

Fig. 5. Overview of the network accessibility analysis at a given time step *t*.

correspond to the 5% and 95% percentile values). Finally, the methodology presented in Fig. 5 is repeated for any relevant pairs of OD nodes and for each time step of the storm scenario to obtain the time evolution of the accessibility of NaTech events and petrochemical facilities, as illustrated in the next sections for a case study area.

3. Case study area and storm surge scenarios

As a proof of concept, the integrated framework proposed in the previous sections is demonstrated for a case study area located along the Houston Ship Channel (HSC), in Texas, US; an aerial view of the case study area is shown in Fig. 6a. As observed in this figure, the case study area comprises a major refinery with 421 ASTs, surrounded by a city with a population of approximately 76,000 people. This area was specifically chosen because both the urban area and refinery could be subjected to extensive storm surge during severe hurricanes, and because the road network is sufficiently developed to adequately illustrate the integrated framework.

3.1. Data collection and road network development

In order to develop the road network for the case study area, road centerlines were obtained from the 2016 Southeast Texas Addressing and Referencing Map (STAR*Map) database [39]. The locations of bridges in the transportation network were obtained from the National Bridge Inventory database [40], while the geometry and design details of each bridge were obtained from personal communications with the Texas Department of Transportation (TxDOT). The locations of fire stations, which are assumed to be the emergency responders in case of a NaTech event, were identified from the Houston-Galveston Area Council (HGAC) GIS datasets [41]. The major neighborhoods where refinery workers could reside were identified from aerial imagery and the census block groups dataset developed by the US Census Bureau [42]. The locations, geometry, and design of ASTs in the case study area were obtained from Bernier et al. [28]. Lastly, the elevations of each road, bridge, and AST were obtained from the HGAC LiDAR Imagery [38].

An overview of the resulting road network for the case study area is shown in Fig. 6b; in its undisrupted form, the network is composed of 167 links and 111 nodes, of which 31 are bridges and 3 are fire stations. To limit the computational cost of the network analysis and demonstrate the concept, the road network is only composed of the highways and major roads in the urban area as well as the main access roads of the refinery. Once the potential NaTech sites are identified, additional links and nodes will also be introduced to connect these sites to the road network as detailed in Section 4.1. Based on the STAR*Map database [39] and accounting for adverse driving conditions in a storm, a mean vehicle speed of 50 mph (80 km/h) is used for highways, while a value of 20 mph (32 km/h) is assumed for all other roads. As discussed previously, the vehicle speed is modeled as a truncated normal with a standard deviation of 5 mph (8 km/h).

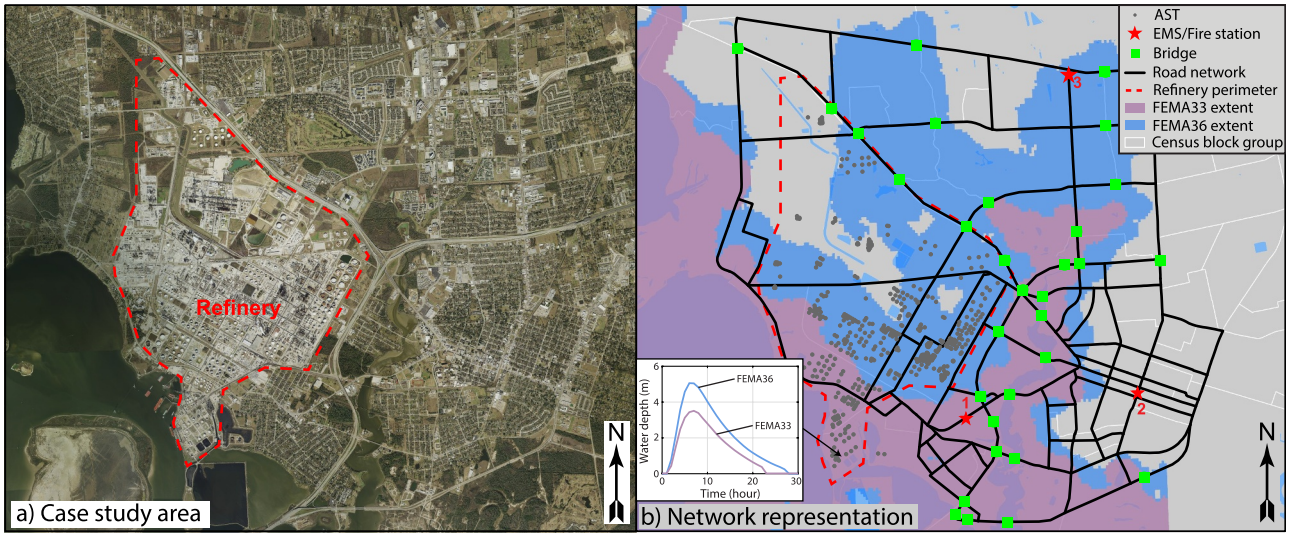

Fig. 6. (a) Aerial imagery of the case study area (source: [38]); and (b) network representation of the case study area and maximum extent of the two surge scenarios.

3.2. Storm surge scenarios

To showcase the application of the framework, two storm scenarios of increasing intensity are considered. The two storms are synthetic storms developed by the Federal Emergency Management Agency (FEMA) for its Flood Insurance Study (FIS) of the Texas Coast [43] and are commonly referred to as FEMA033 and FEMA36 storms. According to the statistical analysis presented in Ebersole et al. [44], storms FEMA33 and FEMA36 produce surge levels with a return period of 100- and 500-year in the case study area. Both synthetic storms were modeled and simulated with *ADCIRC + SWAN* by the SSPEED Center at Rice University [45]. Surge and wave conditions were output at every 1-h time step for each storm scenario to determine the time-evolving loads acting on ASTs and bridges and water depth on road segments of the network. The maximum surge extent for both storms is shown in Fig. 6b, along with an example of the time evolution of surge levels in the area. The surge levels in the case study area vary between 0 and 4 m for the 100-year storm surge scenario, while they vary between 0 and 6 m for the 500-year scenario; for both scenarios, storm surge lasts for approximately a day.

4. Results and discussions

4.1. Vulnerability assessment of ASTs and bridges in the case study area

For both storm scenarios, vulnerability assessments of ASTs and bridges in the case study area are performed using the methodologies outlined in Sections 2.4. and 2.5. to determine the locations of NaTech events and evaluate network disruptions due to bridge failures. Results of the vulnerability assessments are summarized in Fig. 7. This figure shows the probability of failure of each AST and bridge when peak storm surge occurs in the case study area (i.e., $t = 7$ h for FEMA33 and $t = 6$ h for FEMA33). From Fig. 7, it is possible to identify a cluster of vulnerable ASTs where NaTech events could occur during both storm scenarios. An additional link in the road network, shown in red in Fig. 7, was introduced to allow emergency responders to access this area. Based on the time-evolving probabilities of failure, Table 1 also indicates the time periods when emergency responders might need to respond to a NaTech event at this location; as most ASTs have a fairly similar geometry and are subjected to similar surge levels, it was possible to identify a single time period per storm scenario for this group of vulnerable ASTs. As further detailed in the next section, most vulnerable bridges are located along a major waterway crossing the area.

Table 1
Time period when NaTech events are likely to occur in the case study area.

Storm scenario	Time since beginning of storm scenario (hours)		
	Start	End	Most likely point in time
FEMA33 (100-yr)	4	12	7
FEMA36 (500-yr)	3	16	6

4.2. Accessibility analysis of the case study area

With the above vulnerability assessments of ASTs and bridges in the case study area, it is now possible to: (i) assess the accessibility of the NaTech site identified in Section 4.1. to emergency responders; and (ii) determine the post-storm accessibility of the refinery to workers required to repair critical infrastructure and restart operations. First, to illustrate how both storm scenarios disrupt the entire road network, Fig. 8 shows the time evolution of the mean operational path ratio with 90% confidence bounds. As expected, the 500-year storm scenario induces more severe disruptions in the road network; at peak surge, only 15% of the network is operable, compared to 62% for the 100-year scenario. Fig. 8 also illustrates the importance of considering the structural vulnerability of bridges when performing the network accessibility analysis. While the effect of bridge failures is minimal before peak surge, it can significantly affect accessibility when storm surge recedes. When no bridge failures are considered, the operational path ratios go back to almost 100% at the end of the storms; the operational path ratios do not return exactly to 100% as some low-lying areas remain flooded even when storm surge has receded. However, when bridges fail, it is not possible to return to such high ratios; bridges remain in a failed state, and the network is disrupted until they are repaired. Moreover, the effects of uncertainties (i.e., inundation threshold (Θ) and bridge failure), while limited for the 100-year scenario, are significant for the 500-year scenario; wide confidence bounds can be observed in Fig. 8b. Such wide confidence bounds are due to the larger impacted area and disruptions caused by the 500-year scenario, and the probabilistic nature of bridge and road closures; given the sparsity of the case study network, the removal (or not) of a single link in the network can significantly affect the total number of operable paths [46]. The effect of uncertainties is also more important after peak surge because the surge recedes slowly, while it rises quickly. Lastly, confidence bounds are wider when bridge failures, which are an additional source of randomness, are considered.

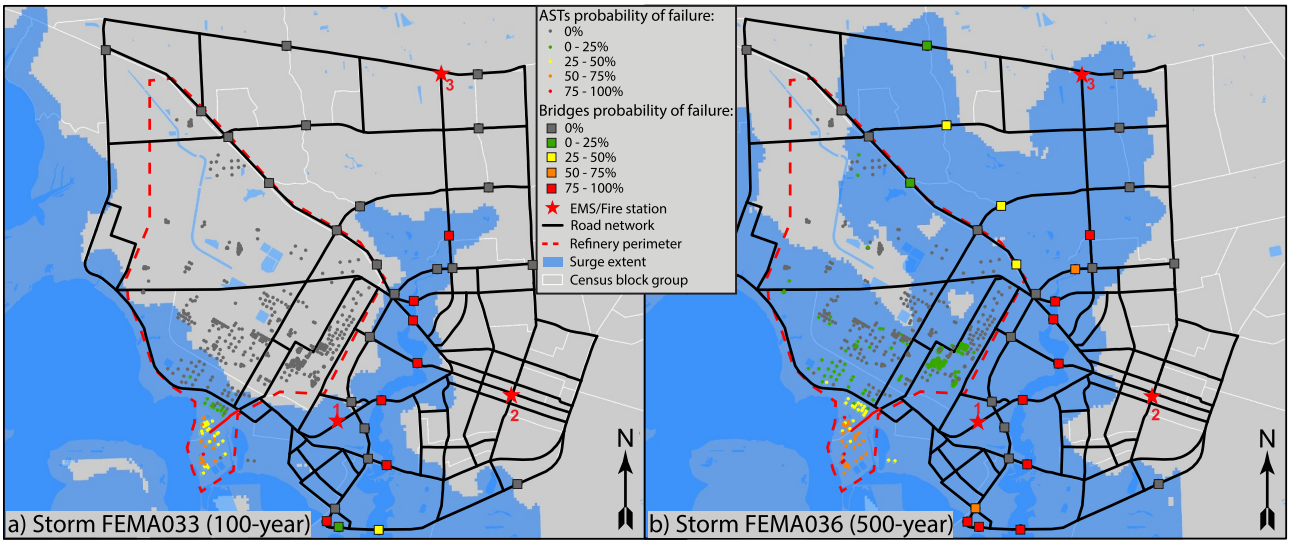

Fig. 7. Vulnerability of ASTs and bridges in the case study area for storms: (a) FEMA33; and (b) FEMA36. The probabilities correspond to the time when peak storm surge occurs.

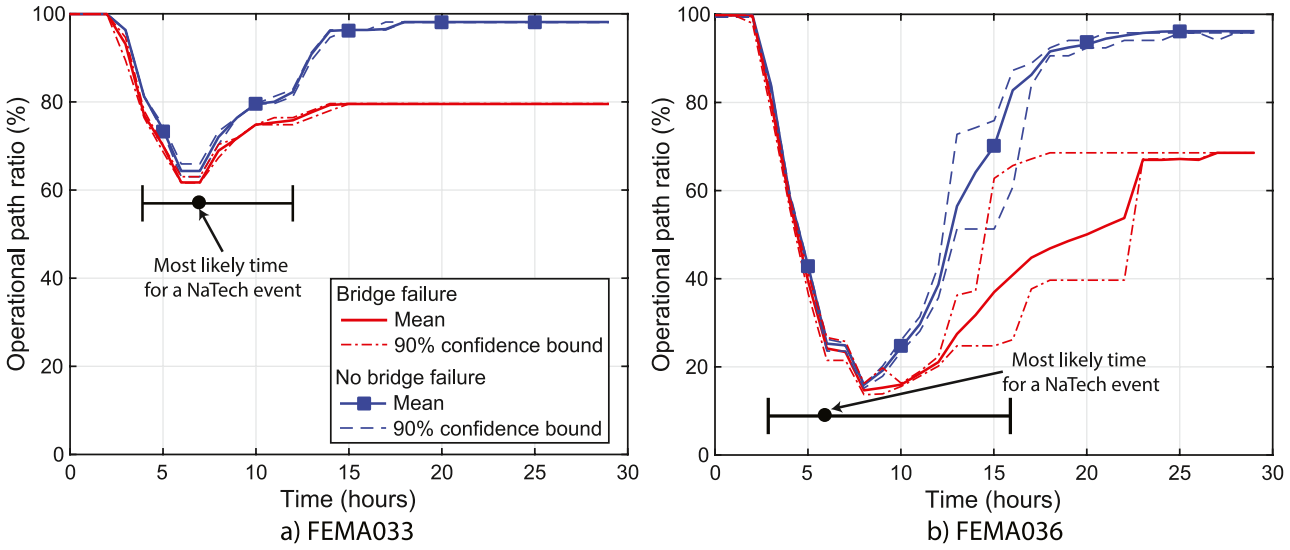

Fig. 8. Evolution of operational path ratios (r) and effects of bridge failures for storm scenarios: (a) FEMA33 (100-year event); and (b) FEMA36 (500-year event).

4.2.1. Emergency service accessibility in case of a NaTech event

Results presented in Fig. 8 also indicate that the most severe disruptions in the road network happen during the same time periods, previously identified in Table 1, in which AST failures and NaTech events are likely to occur in the case study area. However, Fig. 8 provides limited information regarding the actual accessibility of the NaTech events to emergency responders. Thus, the four metrics presented in Section 2.6. – connectivity loss, probability of non-connectivity, travel time, and travel distance – are plotted in Figs. 9–11 to quantify the accessibility between the fire stations identified in Section 3.1. and the NaTech site identified in Section 4.1. during both storm scenarios. All figures present the mean metrics and 90% confidence bounds. Results are only presented for fire stations #2 and #3 (see Fig. 2b); fire station #1 is not considered because it is subjected to more than 1 and 2 m of inundation during the 100-year and 500-year scenarios respectively and would likely not be operational during the storms.

Fig. 9 shows the time evolution of connectivity loss between fire stations and the NaTech site. For the 100-year storm scenario, there is no connectivity loss for fire station #3, while connectivity loss increases to 35% for fire station #2 and remains relatively constant for the rest of the storm. From Eq. (8), this indicates that the distance to reach the NaTech site from fire station #2 increased by approximately 50%. As observed in Fig. 7a and detailed below, bridge failures between the refinery and fire station #2 are the main source of network disruption; road inundations mainly occur in the vicinity of the failed bridges. In addition, the probability of non-connectivity for both fire stations is null for the entire duration of the storm. Thus, the location of NaTech events remains accessible to emergency responders at all times during the 100-year scenario.

For the 500-year scenario, the connectivity loss is more severe, as shown in Fig. 9b. Connectivity loss quickly reaches 100% at $t = 5$ h for both fire stations, and the NaTech site remains completely inaccessible until $t = 12$ h; during that period, all access roads to the refinery are flooded by more than 0.75 m of water. A similar trend is observed in Fig. 10, which shows the time evolution of probability of non-connectivity between fire stations and the NaTech site for the 500-year storm scenario. The probability of non-connectivity has a value of 1.0 between $t = 5$ and 12 h, and only reaches values close to zero after $t = 23$ h. Even though the probability of non-connectivity is null at the end of the storm, the mean connectivity loss of fire station #2 is still

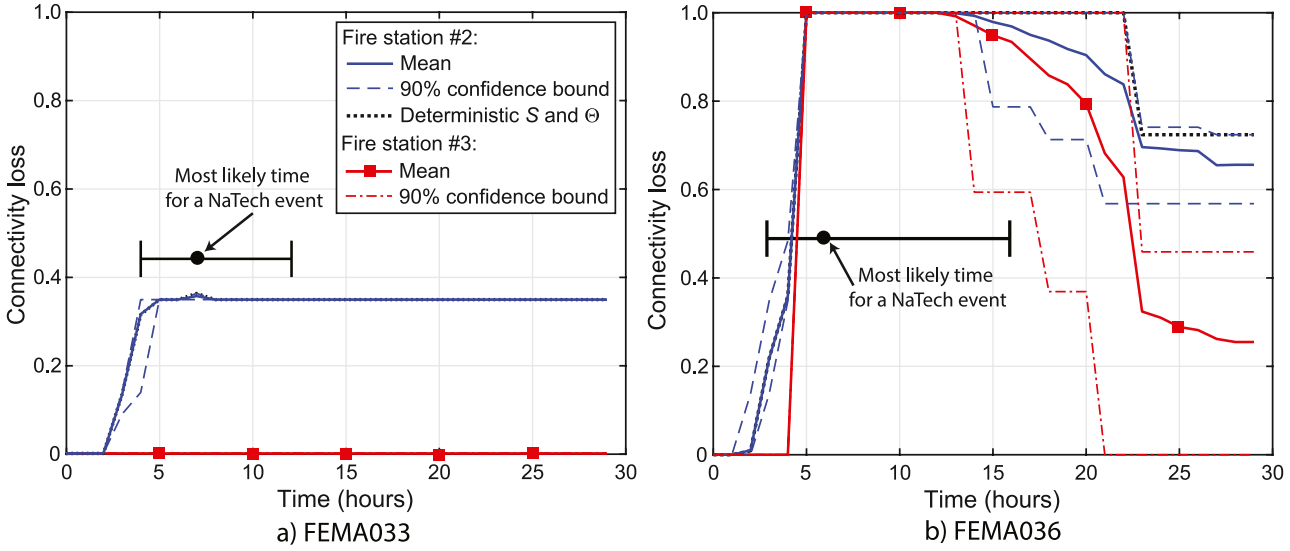

Fig. 9. Evolution of connectivity loss ($CL_{O\to D}$) between fire stations and NaTech site for storm scenarios: (a) FEMA33 (100-year event); and (b) FEMA36 (500-year event).

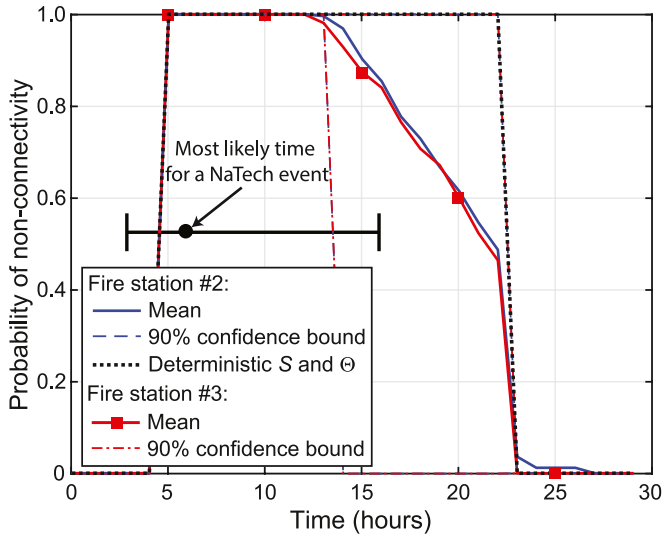

Fig. 10. Evolution of probability of non-connectivity ($P_{f,\ O\to D}$) between fire stations and NaTech site for storm scenario FEMA36 (500-year event).

relatively high with a value of 65%, as shown in Fig. 9b. As detailed below, a large number of failed bridges significantly affect the connectivity between this station and the NaTech site. The mean connectivity loss of fire station #3, which is less affected by bridge failures, is 25% at the end of the storm. Results from Figs. 9b and 10 indicate that the NaTech site would be inaccessible or hardly accessible, with mean probability of non-connectivity above 0.8, during most of the time period when an AST failure and NaTech event could occur. Even after that time period, the site could be hardly accessible until $t = 22$ h, when both the mean connectivity loss and the mean probability of non-connectivity significantly decrease. Thus, the NaTech site could be inaccessible or hardly accessible for a period of 17 h, which would significantly hinder mitigation and emergency activities in case of an AST failure and NaTech event during the 500-year scenario.

Fig. 11 shows the time evolution of travel time and travel distance between fire stations and the NaTech site for both storm scenarios. To better understand Fig. 11, Fig. 12 illustrates the quickest routes between fire stations and the NaTech site before and after each storm and also shows bridges with a high probability of being in a failed state at the end of the storm scenarios (i.e. $p_f^{(t=29)} > 0.75$). The quickest route after a storm shown in Fig. 12 corresponds to the mode route (i.e., the most frequent route from the MCS samples). As expected, for the 100-year scenario, the route between fire station #3 and the NaTech site is not affected by storm surge. However, after peak surge, increases in travel time and distance are observed for fire station #2 as emergency responders from this station need to detour around the failed bridges, as shown in Fig. 12. For the 500-year scenario, Fig. 11b shows a gap corresponding to the time period when the probability of non-connectivity is equal to 1.0. Additionally, the mean travel time and distance are computed only for the MCS samples for which there exists a path between the fire stations and the NaTech site. This explains the tight confidence bounds right after the gap in Fig. 11b, because there are very few samples for which such a path exists between $t = 13$ and 16 h. At the end of the 500-year scenario, mean travel time and distance increase by a factor of 3.0 and 1.5 for fire station #2 and #3 respectively. These factors can reach values up to 4.7 and 2.5 respectively during the storm, further highlighting the fact that the site could be difficult to access in case of a NaTech event. Furthermore, after peak surge, it is possible to observe that on average fire station #3 has the shortest travel time and distance to the NaTech site, even though it had the longest travel time and distance prior to the storm. As shown in Fig. 12, emergency responders from station #2 would first need to reach station #3 before reaching the NaTech site due to bridge failures. In the absence of accessibility analysis, responders from station #2 are likely to be the ones dispatched to the NaTech site given their geographical proximity. Thus, the results of the network accessibility analysis are valuable to efficiently manage and dispatch emergency resources, which may be limited during a storm, in case of a NaTech event. It is worth mentioning that the results presented in Fig. 11 are best-case estimates since the shortest-path approach in the network analysis assumes that emergency responders are perfectly aware of disruptions when travelling on the network. During a real-time storm event, it is unlikely that emergency responders would be fully informed

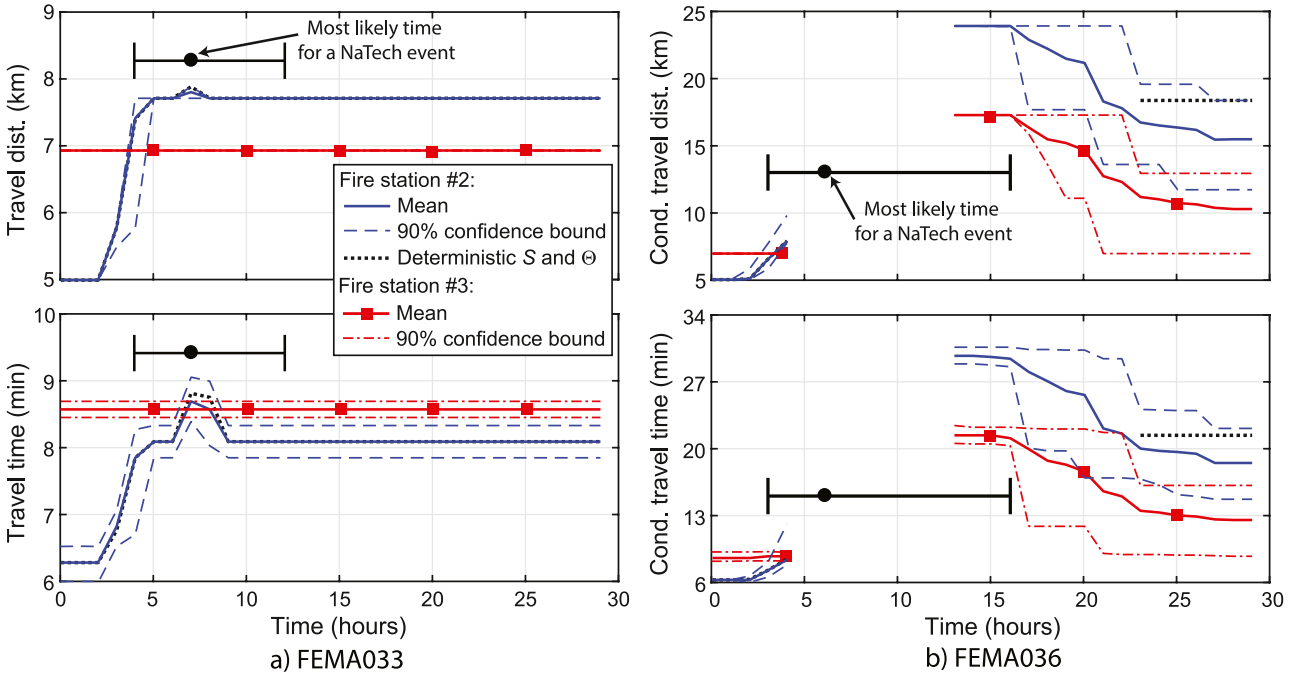

Fig. 11. Evolution of travel time ($T_{O\to D}$) and travel distance ($L_{O\to D}$) between fire stations and NaTech site for storm scenarios: (a) FEMA33 (100-year event); and (b) FEMA36 (500-year event).

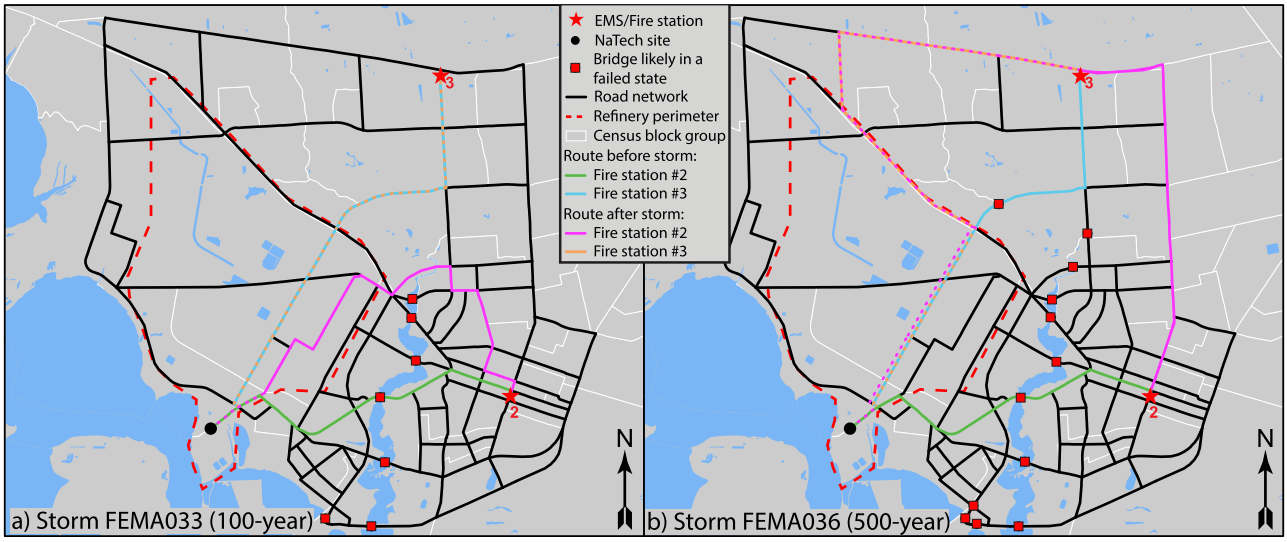

Fig. 12. Quickest routes between fire stations and NaTech site before ($t = 0$ h) and after ($t = 29$ h) for storm scenarios: (a) FEMA33 (100-year event); and (b) FEMA36 (500-year event). The quickest route shown after a storm is the mode route.

and prepared for network disruptions, potentially yielding greater travel times and distances. The consideration of such uncertainties in the network analysis offer interesting opportunities for future research.

In Figs. 9–11, wide confidence bounds are observed for the 500-year scenario. As all access roads to the refinery are severely inundated in this scenario, the opening or closure of an access road can significantly affect the shortest path (or the existence of such path), resulting in wide confidence bounds. For the 100-year scenario, confidence bounds are tighter as multiple access roads to the refinery remain open at all times. Furthermore, Figs. 9–11 also present a comparison between the probabilistic network analysis and a deterministic analysis where the inundation threshold (Θ) and vehicle velocity (S) are kept constant at their mean values; the comparison is shown for fire station #2 only. For the 100-year scenario, both probabilistic and deterministic analyses provide similar results, highlighting the relative insignificance of considering sources of uncertainty for this scenario. However, for the 500-year scenario, the deterministic analysis almost corresponds to the upper confidence bounds of the probabilistic analysis, and a larger time period of complete loss of accessibility to the NaTech site is predicted. In the deterministic analysis, a road only becomes operational again when the water depth is strictly less than 0.6; however, in the probabilistic analysis, the road could become operational earlier depending on the distribution of Θ, resulting in lower mean connectivity metric values. This is of significance for the 500-year scenario as several access roads to the refinery have water depths slightly above 0.6 m between $t = 12$ and 23 h. Thus, for this specific scenario, neglecting the uncertainties associated with Θ and S yields conservative results for the accessibility analysis compared to the mean values of the probabilistic analysis. Finally, the wide confidence bounds observed for the 500-year scenario also highlight the future need to adequately quantify these sources of uncertainty; the distributions used in this paper are adopted as an illustrative example given the current lack of information.

Overall, the above results for the case study area demonstrate that the integrated framework is an efficient tool to evaluate the accessibility of potential NaTech events to emergency responders during and after storm events. The integrated framework can provide useful information such as the level of network disruption when a NaTech event could occur, the likelihood and ability to reach such NaTech events, the routes that should be used to access these events, the confidence levels regarding the accessibility of these events, and the emergency resources that should be prioritized. In turn, this information can provide for better emergency and mitigation planning to potentially reduce the impacts of a NaTech event during severe storm surge events.

4.2.2. Worker accessibility after a storm surge event

The proposed integrated framework is also employed to evaluate the accessibility of the refinery to workers in order to repair critical infrastructure and restart operations after a storm. As mentioned earlier, this issue was reported by industry managers following recent storms in the Gulf Coast [12]. Since the exact locations of workers in the case study area are unknown, the accessibility analysis is performed at the neighborhood level. The different residential neighborhoods where refinery workers may live were delineated using the US Census block groups (BGs); BGs are a geographical unit with a population ranging between 600 and 3000 people and are commonly used as proxies for neighborhoods [16]. Using aerial imagery, the road network nodes closest to the main residential areas in each of the BGs were then identified. A node central to the refinery was also employed to assess connectivity, as shown in Fig. 13. The network accessibility analysis was then performed to assess the connectivity between each node representing a residential neighborhood and the refinery at the end of the storm scenarios. Severely flooded neighborhoods during a storm (i.e., neighborhoods with more than 1.0 m of inundation) were excluded from the analysis, given potential of evacuated residents or personal hardships that may preclude these residents from immediately returning to work [47,48].

Results of the accessibility analysis between residential neighborhoods and the refinery are shown in Fig. 13; results are only shown for the 500-year storm scenario as limited insight was obtained from the 100-year scenario. Fig. 13a presents the mean connectivity loss ($\overline{CL}_{O\to D}^{(t=29)}$) between each neighborhood and the refinery after the storm, while Fig. 13b shows the mean travel time increase ratio ($\overline{TI}_{O\to D}$) after the storm. The travel time increase ratio is defined as $\overline{TI}_{O\to D} = \overline{T}_{O\to D}^{(t=29)} / \overline{T}_{O\to D}^{(t=0)}$. While the probability of non-connectivity to the refinery is null for all neighborhoods after the storm, certain neighborhoods suffered significant connectivity loss as observed in Fig. 13a. Before the storm, workers in the neighborhoods located east of the refinery were the closest ones to the refinery. However, after the storm, the travel distance to reach the refinery increased significantly for these workers due to bridge failures; connectivity loss reaches values up to 0.8 for the neighborhoods located east of the refinery. This also resulted in travel time increases by a factor up to 3.8 for these neighborhoods, as shown in Fig. 13b. On average, after the storm, travel times for workers located north of the refinery are 5–15 min shorter than for workers located east. Before the storm, workers located east of the refinery could reach the refinery up to 5 min before workers located to the north. Moreover, this comparison assumes that workers know exactly

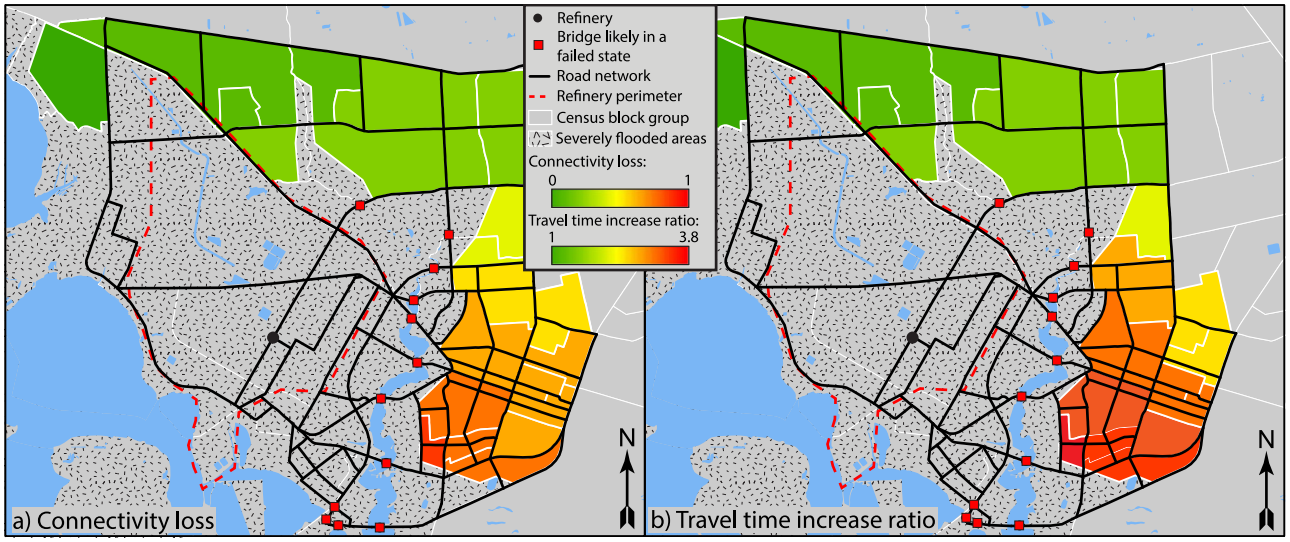

Fig. 13. (a) Mean connectivity loss ($\overline{CL}_{O\to D}^{(t=29)}$); and (b) mean travel time increase ratio ($\overline{TI}_{O\to D}$) between worker neighborhoods and the refinery at the end (t = 29 h) for storm scenario FEMA36 (500-year event).

which route to take to reach the refinery. While route changes are minor for workers located north of the refinery, they are significant for workers located to the east; it is unlikely that these workers would be fully aware of these changes, potentially resulting in further accessibility issues. As some facilities request essential or emergency designated workers to live within a certain radius of the facility, the above results suggest that such workers may not necessarily be in the best position to access the facility after a storm compared to workers living further away. The overall network topology, water crossing features, infrastructure vulnerability and hazard potential play an important role in determining ideal proximity. Thus, the integrated framework offers valuable information to better manage personnel and critical activities following a severe storm.

5. Summary and conclusions

This study developed an integrated framework to efficiently evaluate the accessibility of potentially vulnerable petrochemical facilities, where NaTech events could occur, to emergency responders and facility workers during and after a storm surge event. First, storm surge modeling was coupled with AST fragility models to determine the potential location of NaTech events and the time period when NaTech events are likely to occur during a storm scenario. Then, coastal bridge fragility models and GIS analysis were employed to determine road network disruptions such as bridge failures and road inundations. Finally, a probabilistic network analysis was performed to propagate uncertainties associated with the network disruptions and to quantify the time evolution of select accessibility metrics. As a proof of concept, the proposed framework was applied to a case study area and petrochemical facility in Texas, and for two synthetic storm scenarios of increasing intensity. The integrated framework was first employed to determine the time-evolving accessibility of NaTech events to emergency responders and then to evaluate the accessibility of the case study petrochemical facility to workers in order to repair critical infrastructure and restart operations after a storm.

Results of the accessibility analysis highlighted the importance of considering the structural vulnerability of critical transportation infrastructure during flood or storm surge events. Results showed that considering the potential for bridge failures is critical to obtaining a realistic time evolution of road network accessibility and recovery. Only accounting for road inundations, as previous studies have done, can significantly underestimate network disruptions when storm surge recedes. In turn, this can lead to inaccurate network accessibility and recovery assessments. Moreover, the results presented here revealed the importance of considering and propagating the sources of uncertainty associated with network disruptions in the analysis. Performing a deterministic network analysis was shown to provide overly conservative accessibility results for the scenarios considered, and furthermore, the lack of insight on confidence levels can undermine the value of such results for practical decision-making purposes. The effects of uncertainties were also found to be primarily significant for severe storm surge scenarios for which major disruptions in the road network are expected including bridge failures, while they were negligible for smaller storm surge events with a smaller geographic footprint and more limited network disruptions.

With respect to findings for case study area, the framework provided useful insights, such as the level of network disruption during the time period when NaTech events are likely to occur; the likelihood, travel time, and travel distance to reach the NaTech events; and the confidence levels regarding the accessibility results. Results indicated that the accessibility of the case study facility is highly restricted during severe storm surge events. During a 500-year scenario, the location of NaTech events at the facility could be inaccessible or hardly accessible for almost 20 h, thereby significantly affecting mitigation and emergency activities to limit the potential impacts of such NaTech events. However, results also demonstrated that during less severe storm events, such as a 100-year scenario, emergency responders would have continuous and almost unaffected access to the location of potential NaTech events. Furthermore, results of the accessibility analysis indicated that the fire stations located closest to the petrochemical facility were not necessarily the best suited to access the NaTech site. Due to network disruptions, especially bridge failures, fire stations located further away might have better connectivity and shorter travel times than the closest stations. Similar findings were also obtained for the post-storm accessibility of the facility to workers, highlighting the benefits of the proposed framework to better manage personnel and emergency resources, which are both often limited during and after a severe storm.

Overall, the results and findings presented here demonstrate that the proposed integrated framework offers a powerful tool to identify the locations of potential NaTech events, determine the potential for road network disruptions, and evaluate the accessibility of potential NaTech events to emergency responders and workers during and after storm events. The integrated framework can provide useful insights to industry managers and decision makers in order to improve risk assessment and emergency planning before a storm, facilitate mitigation

and emergency activities during a storm, manage resources and personnel more efficiently, and ultimately reduce the potential impacts of NaTech events during and after a storm. A limitation of this study is the use of deterministic and synthetic storm surge scenarios in the illustrative cases. Future work will improve the proposed methodology by considering the uncertainties associated with storm surge modeling and prediction, and by coupling the integrated framework with real-time surge prediction tools (i.e. [49]) to provide accessibility data to industry managers before and during actual storm surge events. Finally, future work will also include the effects of sources of uncertainties regarding behavioral factors and disruption awareness, as well as additional sources of disruptions such as the structural vulnerability of roadways and the effects of debris.

Acknowledgments

The authors gratefully acknowledge the support of this research by the National Science Foundation under awards CMMI-1635784 and OISE-1545837, the Rice University Shell Center for Sustainability, and the Houston Endowment via the SSPEED Center at Rice University. The contributions of the first author were also supported in part by the Natural Sciences and Engineering Research Council of Canada. The authors thank Benjamin Bass for providing the *ADCIRC + SWAN* results. Any opinions, findings, and conclusions or recommendations expressed in this paper are those of the authors and do not necessarily reflect the views of the sponsors.

References

[1] Sengul H, Santella N, Steinberg LJ, Cruz AM. Analysis of hazardous material releases due to natural hazards in the United States. Disasters 2012;36:723–43.
[2] Santella N, Steinberg LJ, Sengul H. Petroleum and hazardous material releases from industrial facilities associated with Hurricane Katrina. Risk Anal 2010;30:635–49.
[3] Bernier C, Padgett JE. Forensic investigation of aboveground storage tank failures during Hurricane Harvey using fragility models. Forensic Eng. 8th Congr. 2018.
[4] Palinkas L, Downs M, Petterson J, Russell J. Social, cultural, and psychological impacts of the Exxon Valdez oil spill. Hum Organ 1993;52:1–13.
[5] Landucci G, Antonioni G, Tugnoli A, Cozzani V. Release of hazardous substances in flood events: damage model for atmospheric storage tanks. Reliab Eng Syst Saf 2012;106:200–16.
[6] Khakzad N, Van Gelder P. Vulnerability of industrial plants to flood-induced natechs: a Bayesian network approach. Reliab Eng Syst Saf 2018;169:403–11.
[7] Cruz AM, Okada N. Methodology for preliminary assessment of Natech risk in urban areas. Nat Hazards 2008;46:199–220.
[8] Krausmann E. Natural hazard triggered technological (Natech) accidents—an overlooked type of risk ? Loss Prev Bull 250 2016:11–5.
[9] Galderisi A, Ceudech A, Pistucci M. A method for Na-tech risk assessment as supporting tool for land use planning mitigation strategies. Nat Hazards 2008;46(2):221–41.
[10] Cruz AM, Krausmann E. Vulnerability of the oil and gas sector to climate change and extreme weather events. Clim Change 2013;121:41–53.
[11] Eaton C, Blum J. Galena park gasoline spill dwarfed other Harvey leaks, but stayed out of public eye for days. Houst Chron 2017https://www.houstonchronicle.com/business/article/Galena-Park-gasoline-spill-dwarfed-other-Harvey-12192956.php.
[12] American Fuel & Petrochemical Manufacturers. Hurricane lessons learned from Harvey. AFPM 2018 annu. meet. 2018.
[13] Coles D, Yu D, Wilby RL, Green D, Herring Z. Beyond 'flood hotspots': modelling emergency service accessibility during flooding in York, UK. J Hydrol 2017;546:419–36.
[14] Green D, Yu D, Pattison I, Wilby R, Bosher L, Patel R, et al. City-scale accessibility of emergency responders operating during flood events. Nat Hazards Earth Syst Sci 2017;17(1):1–16.
[15] Yin J, Yu D, Lin N, Wilby RL. Evaluating the cascading impacts of sea level rise and coastal flooding on emergency response spatial accessibility in Lower Manhattan, New York City. J Hydrol 2017;555:648–58.
[16] Gori A, Gidaris I, Elliott JR, Padgett J, Loughran K, Bedient P, et al. Accessibility and recovery assessment of Houston's roadway network due to fluvial flooding during Hurricane Harvey. Nat Hazards Rev 2019. (In review).
[17] Santella N, Steinberg LJ, Aguirra GA. Empirical estimation of the conditional probability of NaTech events within the United States. Risk Anal 2011;31:951–68.
[18] Cozzani V, Campedel M, Renni E, Krausmann E. Industrial accidents triggered by flood events: analysis of past accidents. J Hazard Mater 2010;175(, 1–3):501–9.
[19] Padgett J, DesRoches R, Nielson B, Yashinsky M, Kwon O-S, Burdette N, et al. Bridge damage and repair costs from Hurricane Katrina. J Bridg Eng 2008;13:6–14.
[20] Ataei N. Vulnerability assessment of coastal bridges subjected to hurricane events. Rice University; 2013.
[21] Anarde KA, Kameshwar S, Irza JN, Nittrouer JA, Lorenzo-trueba J, Padgett JE, et al. Impacts of hurricane storm surge on infrastructure vulnerability for an evolving coastal landscape. Nat Hazards Rev 2018;19:04017020.
[22] National Weather Service. Turn around don't drown 2015. http://www.nws.noaa.gov/os/water/tadd/ (Accessed August 8, 2018).
[23] Dietrich JC, Tanaka S, Westerink JJ, Dawson CN, Luettich RA, Zijlema M, et al. Performance of the unstructured-mesh, SWAN + ADCIRC model in computing hurricane waves and surge. J Sci Comput 2012;52:468–97.
[24] Hope ME, Westerink JJ, Kennedy AB, Kerr PC, Dietrich JC, Dawson C, et al. Hindcast and validation of Hurricane Ike (2008) waves, forerunner, and storm surge. J Geophys Res Ocean 2013;118:4424–60.
[25] ESRI. ArcGIS 10.5 2016.
[26] Godoy L. Performance of storage tanks in oil facilities damaged by Hurricanes Katrina and Rita. J Perform Constr Facil 2007;21:441–9.
[27] Kameshwar S, Padgett JE. Storm surge fragility assessment of above ground storage tanks. Struct Saf 2018;70:48–58.
[28] Bernier C, Elliott JR, Padgett JE, Kellerman F, Bedient PB. Evolution of social vulnerability and risks of chemical spills during storm surge along the Houston Ship Channel. Nat Hazards Rev 2017;18:1–14.
[29] Masoomi H, Van De Lindt JW, Ameri MR, Do TQ, Webb BM. Combined wind-wave-surge hurricane-induced damage prediction for buildings. J Struct Eng 2018;145:1–15.
[30] Stearns M, Padgett JE. Impact of 2008 Hurricane Ike on bridge infrastructure in the Houston/Galveston region. J Perform Constr Facil 2012;26:441–52.
[31] Balomenos GP, Kameshwar S, Padgett JE. Parameterized fragility models for multi-bridge classes subjected to hurricane loads. J Bridg Eng 2019 (In review).
[32] Ross SM. Stochastic Processes. 2nd ed. John Wiley & Sons; 1996.
[33] Elfrink B, Hanes DM, Ruessink BG. Parameterization and simulation of near bed orbital velocities under irregular waves in shallow water. Coast Eng 2006;53:915–27.
[34] Newman A. Networks: an introduction. Oxford University Press; 2010.
[35] Zuev KM, Wu S, Beck JL. General network reliability problem and its efficient solution by subset simulation. Probabilistic Eng Mech 2015;40:25–35.
[36] Pollack M, Wiebenson W. Solutions of the shortest-route problem—a review. Oper Res 1960;8:224–30.
[37] Dijkstra EW. A note on two problems in connexion with graphs. Numer Math 1959;1:269–71.
[38] Houston-Galveston Area Council. Aerial imagery. http://www.h-gac.com/rds/imagery/aerial-imagery.aspx; 2018, Accessed date: 7 March 2018.
[39] Houston-Galveston Area Council. STAR*Map. http://www.h-gac.com/rds/GIS_Data/starmap/default.aspx; 2018, Accessed date: 7 March 2018.
[40] Federal Highway Administration. National Bridge Inventory (NBI). https://www.fhwa.dot.gov/bridge/nbi.cfm; 2018, Accessed date: 7 March 2018.
[41] Houston-Galveston Area Council. GIS datasets. http://www.h-gac.com/rds/gis-data/gis-datasets.aspx; 2018, Accessed date: 7 March 2018.
[42] US Census Bureau. Cartographic boundary shapefiles—block groups. https://www.census.gov/geo/maps-data/data/cbf/cbf_blkgrp.html; 2018, Accessed date: 7 March 2018.
[43] Federal Emergency Management Agency. Flood insurance study—Harris County, Texas and incorporated areas. Preliminary study 48201CV001A. 2013.
[44] Ebersole BA, Massey TC, Melby JA, Nadal-Caraballo NC, Hendon DL, Richardson TW, et al. Interim report - Ike Dike concept for reducing hurricane storm surge in the Houston-Galveston region. Jackson, MS: Jackson State University; 2016.
[45] Center SSPEED. Severe Storm Prediction, Education, & Evacuation from Disasters Center. http://www.sspeed.rice.edu/; 2018, Accessed date: 7 March 2018.
[46] Vishnu N, Kameshwar S, Padgett J. A framework for resilience assessment of highway transportation networks. In: Gardoni P, editor. Handb. sustain. resilient infrastruct. Syst. editorRoutledge; 2018.
[47] Bourque LB, Siegel JM, Kano M, Wood MM. Weathering the storm: the impact of hurricanes on physical and mental health. Ann Am Acad Pol Soc Sci 2006;604:129–51.
[48] Reininger BM, Raja SA, Carrasco AS, Chen Z, Adams B, McCormick J, et al. Intention to comply with mandatory hurricane evacuation orders among persons living along a coastal area. Disaster Med Public Health Prep 2013;7:46–54.
[49] Louisiana State University. CERA—Coastal Emergency Risks Assessment. https://cera.coastalrisk.live/; 2018, Accessed date: 4 September 2018.